Editors' Suggestion | Featured in Physics

Wave-Function Tomography of Topological Dimer Chains with Long-Range Couplings

F. Pellerin,[1] R. Houvenaghel,[2] W. A. Coish,[3] I. Carusotto,[4] and P. St-Jean[1,5]
[1]Département de Physique, Université de Montréal, C.P. 6128, Succursale Centre-Ville, Montréal, Québec H3C 3J7, Canada
[2]Département de Physique, Ecole Normale Supérieure de Lyon, 46 allée d'Italie, F69007 Lyon, France
[3]Department of Physics, McGill University, 3600 rue University, Montreal, Québec H3A 2T8, Canada
[4]Pitaevskii BEC Center, INO-CNR and Dipartimento di Fisica, Università di Trento, via Sommarive 14, I-38123 Trento, Italy
[5]Institut Courtois, Université de Montréal, Montréal, Quebec H2V 0B3, Canada

(Received 5 July 2023; accepted 12 March 2024; published 1 May 2024)

The ability to tailor with a high accuracy the intersite connectivity in a lattice is a crucial tool for realizing novel topological phases of matter. Here, we report the experimental realization of photonic dimer chains with long-range hopping terms of arbitrary strength and phase, providing a rich generalization of the Su-Schrieffer-Heeger model which, in its conventional form, is limited to nearest-neighbor couplings only. Our experiment is based on a synthetic dimension scheme involving the frequency modes of an optical fiber loop platform. This setup provides direct access to both the band dispersion and the geometry of the Bloch wave functions throughout the entire Brillouin zone allowing us to extract the winding number for any possible configuration. Finally, we highlight a topological phase transition solely driven by a time-reversal-breaking synthetic gauge field associated with the phase of the long-range hopping, providing a route for engineering topological bands in photonic lattices belonging to the AIII symmetry class.

DOI: 10.1103/PhysRevLett.132.183802

Introduction.—Engineering materials with specific topological properties requires an acute control over the hybridization of electronic orbitals [1]. As was pioneered by the Haldane model [2], introducing next-nearest-neighbor coupling terms with arbitrary phases strongly enriches the variety of phenomena that can be observed in topological band models [3,4]. Furthermore, such long-range connectivity is expected to facilitate the stabilization of strongly correlated states of matter [5].

The experimental implementation and control of sizable hopping terms extending beyond nearest neighbors is typically not a straightforward task [6]. In usual realizations of lattice models based on condensed matter or ultracold atomic systems, hopping typically occurs via tunneling processes mediated by the spatial overlap of wave functions at different sites and is therefore dominated by short-range processes [7,8].

The situation is very different if we consider lattices extending along synthetic dimensions [9]. Here, one or more spatial coordinates are replaced by some other internal degrees of freedom such as energy or momentum in ultracold atomic gases [10–13], or, in photonic systems, frequency [14,15], angular momentum [16,17], spatial [18] or temporal modes [19,20]. In the specific case of photonic lattices, a wide variety of hopping terms can be engineered [21], which has led to the observation of the four-dimensional quantum Hall effect [22], the non-Hermitian skin effect [23,24], and topological complex-energy braiding features [25]. This enhanced control over the intersite connectivity has also proven to be instrumental to the development of new generations of optical devices, including topological lasers [26], non-Hermitian sensors [27], and photonic networks [28,29].

In this Letter, we use the frequency of the photon modes in an optical fiber loop as a synthetic dimension [15] to experimentally engineer one-dimensional dimerized lattices with full control over the range, magnitude, and phase of the hopping terms. When only nearest-neighbor couplings are present, our lattice realizes the well-known Su-Schrieffer-Heeger (SSH) model [30], which displays two topologically distinct phases associated with the integer-valued winding number $\mathcal{W} = 0, 1$. A wider variety of phases with $\mathcal{W}$ ranging from -1 to $+2$ is realized by adding 3rd-nearest-neighbor hopping terms with specific amplitudes [31–33]. The entire topological phase diagram of this Hamiltonian is reconstructed using a wave-function tomography technique for the Bloch modes. Finally, we report the generation of a time-reversal-breaking synthetic gauge field, which allows to change the band topology without modifying the relative strength of the couplings, in sharp contrast with the conventional SSH model where this is necessary.

The topological model.—We consider in this work one-dimensional dimerized chains that present chiral symmetry, i.e., where sites are identical and hopping processes only connect sites in different sublattices [Fig. 1(a)]. Under the tight-binding approximation, the generic Hamiltonian describing such lattices is

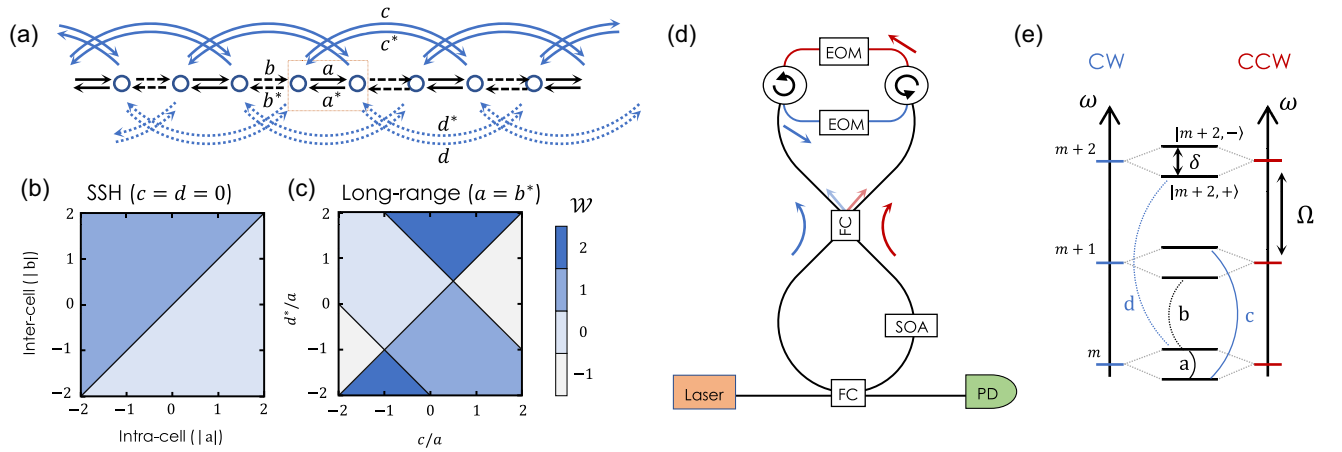

FIG. 1. (a) Schematic representation of a topological dimer chain. The unit cell is defined by the dotted rectangle and the arrows describe the forward- (a, b, c, d) and backward- (a^*, b^*, c^*, d^*) propagating hopping amplitudes. (b)–(c) Topological phase diagrams presenting the winding number as a function of the different couplings for the SSH model (b) and the dimer chain with long-range couplings (c) in a case where $a = b^*$ and the ratios c/a and d^*/a are real. (d) Experimental setup: clockwise (blue) and counterclockwise (red) modes of an optical fiber loop are coupled with a 75:25 fiber coupler. The system is probed with an optical fiber acting as a transmission line weakly coupled to the cavity with a 99:1 FC. On top, circulators are used to independently modulate CW and CCW modes with a pair of electro-optical phase modulators. (e) The energy spectrum of the cavity has a FSR of Ω and consists of symmetric and antisymmetric superpositions of CW and CCW modes ($|m, \pm\rangle$), separated by a frequency splitting δ.

$$H(k) = \begin{pmatrix} 0 & g(k) \\ g^*(k) & 0 \end{pmatrix}, \tag{1}$$

where the off-diagonal term $g(k) = |g(k)|e^{i\phi(k)}$ describes the hopping terms in Fourier space. This Hamiltonian presents band dispersions $E_\pm(k) = \pm|g(k)|$, and a phase difference $\phi(k)$ between the components of the Bloch modes on the two sublattices:

$$|k_\pm\rangle = \frac{1}{\sqrt{2}} \begin{bmatrix} 1 \\ \pm e^{-i\phi(k)} \end{bmatrix}. \tag{2}$$

In this framework, the topological phases are characterized by the number of times $g(k)$ winds around the origin of the complex plane as k spans the Brillouin zone. This quantity, called the winding number $\mathcal{W}$, is linked to the number of edge states present at the boundaries of a finite lattice. Although the winding number depends on the definition of the unit cell and is thus ill defined for infinite lattices, it can be identified unambiguously for finite lattices where the definition of the unit cell is imposed by the chain termination.

When only nearest-neighbor hopping amplitudes are considered, $g(k) = a + b^* e^{+ikl}$ with l the lattice constant. This realizes the SSH model with winding numbers $\mathcal{W} = 0$ and 1 for $|a| > |b|$ and $|a| < |b|$, respectively [Fig. 1(b)]. Adding 3rd-nearest-neighbor hopping terms leads to

$$g(k) = a + b^* e^{+ikl} + c e^{-ikl} + d^* e^{+2ikl}, \tag{3}$$

and the winding number can now take values ranging from -1 to $+2$ upon varying the hopping amplitudes, see Fig. 1(c) for the cases where $a = b^*$, and ratios c/a and d^*/a are real. This is equivalent to a model with real hopping parameters after a gauge transformation $g(k) \to e^{-i\phi_a} g(k)$ with $\phi_a = \arg(a)$ [31].

The synthetic photonic lattice.—In our experiment, we use the frequency of photons confined in an optical fiber loop as a synthetic dimension [34]. The underlying principle of this approach, inspired by Refs. [14,15,35], is to emulate the spatial periodicity of a lattice by exploiting the periodicity in frequency of the cavity spectrum, given by the loop's free spectral range (FSR) $l = \Omega$, and mapping each cavity mode of the loop to a single site of the Hamiltonian. Coupling between specific eigenmodes (representing the hopping parameter) is realized by locally modulating the refractive index of the cavity material with electro-optic phase modulators (EOMs) driven at a frequency equal to the corresponding mode spacing.

In order to create the alternating hopping terms of a dimer chain, it is necessary to engineer a cavity with two different frequency splittings and to drive them independently. To do this, we use a single fiber loop and couple the degenerate clockwise (CW) and counterclockwise (CCW) eigenmodes using a 75:25 optical fiber coupler [see Fig. 1(d)]. The resulting hybridized modes are symmetric and antisymmetric superpositions of the CW and CCW modes: $|m, \pm\rangle = (1/\sqrt{2})(|m, \mathrm{CCW}\rangle \pm |m, \mathrm{CW}\rangle)$, where m is the index of the uncoupled modes. In our setup, the splitting between $|m, \pm\rangle$ is $\delta/2\pi = 3.43$ MHz and the FSR is $\Omega/2\pi = 10.03$ MHz [Fig. 1(e)].

In order to further optimize the coupling efficiency between these eigenmodes, we use a pair of circulators

that spatially separate the CW and CCW modes allowing to independently modulate them. In particular, by driving the EOMs with the same electrical signal amplitude but with a π-phase shift, $V_{\mathrm{CCW}}(t) = -V_{\mathrm{CW}}(t)$, we maximize the coupling between states of opposite parity while suppressing those between states belonging to the same sublattice, hence enforcing chiral symmetry [36].

SSH lattices.—As a first application of our scheme, we realize an SSH Hamiltonian by driving the EOMs with a bichromatic signal $V_{\mathrm{CCW/CW}}(t) = \pm(i/2)(V_a e^{-i\delta t} + V_b e^{-i(\Omega-\delta)t}) + \mathrm{c.c.}$ where $\pm$ accounts for the π phase shift between the two modulators on the CCW and CW paths. This modulation gives rise to effective hopping terms $a = i\eta V_a$ and $b^* = i\eta V_b^*$, where η is related to the electro-optical constant and has units of rad s^{-1} V^{-1} [34].

To measure the band dispersion, we probe the time-resolved transmission of the cavity using a high-bandwidth photodiode while scanning the frequency of a continuous-wave excitation laser around a given symmetric hybridized cavity mode $|\bar{m}, +\rangle$. When the laser is resonant with the $\pm$ synthetic SSH band, the transmitted field intensity consists of a train of pulses with period $T = 2\pi/\Omega$:

$$\frac{I_{pd}^{(\pm)}(t)}{|F|^2} \simeq \left[1 - \frac{\kappa}{2}\mathrm{Re}\left\{\frac{1 \pm e^{-i\delta t}e^{i\phi(k)}}{\gamma/2 - i(\Delta\omega_L \mp |g(k)|)}\right\}\right]\Bigg|_{k=t \bmod T}, \tag{4}$$

where F is the input field amplitude, $\Delta\omega_L$ is the detuning between the laser and the considered hybridized cavity mode, and κ is the input-output coupling strength. We work in a regime where κ is smaller than the total decay rate of the cavity $\gamma = \gamma_i + \kappa - G$ with γ_i the intrinsic loss and G the amplification. As usual in synthetic dimension schemes based on frequency [15], the field at each time t probes the state of effective crystal momentum $k = t \bmod T$ within an effective Brillouin zone of size T [37]: the resonant denominator gives intensity dips whenever the frequency of the SSH state at k matches the one of the incident laser, whereas the numerator describes a slow modulation with frequency δ and phase $\phi(k)$.

This slow modulation arises from the fact that we measure light transmitted from the CCW mode while the Bloch eigenmodes consist of linear superpositions of symmetric and antisymmetric combinations of CW and CCW modes that oscillate at different frequencies, giving a beating at their frequency difference δ in the photodiode signal. Importantly, the phase of this modulation is exactly the relative phase of the sublattice amplitudes in the Bloch modes, allowing experimental access to the phase of the wave function in Eq. (2) at every k point.

Figures 2(a) and 2(b) show the transmitted intensity as a function of time (averaged over multiple Brillouin zones to erase the effect of the modulation) and as a function of the laser detuning for the cases $|a| > |b|$ and $|a| < |b|$,

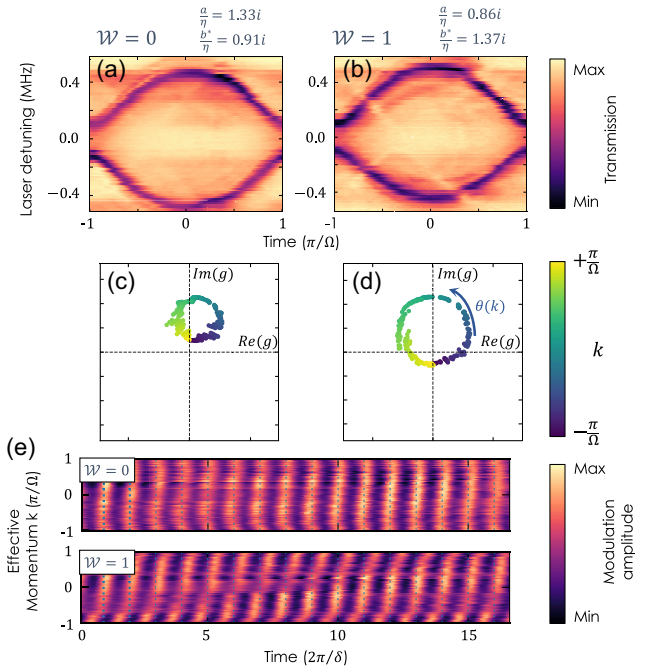

FIG. 2. (a)–(b) Band structure measurements for the trivial (a) and topological phases (b) obtained by probing the transmitted intensity of the cavity as a function of time for different values of the laser detuning. Effective hopping terms (in units of V) are provided above each panel. (c)-(d) Trajectory of $g(k)$ in the complex plane for k moving across the Brillouin zone in the trivial and topological cases exhibiting a winding number $\mathcal{W} = 0$ and 1, respectively. (e) Slow temporal modulation of the amplitude of the transmitted intensity peaks associated with the lower band in the trivial $\mathcal{W} = 0$ (top) and topological $\mathcal{W} = 1$ (bottom) cases. Vertical dashed lines indicate the periodicity of this modulation.

corresponding to the trivial and topological phases of the SSH model. In both cases, we clearly observe the two bands of the SSH Hamiltonian with a well-defined gap, on the order of $E_g \sim 200$ kHz for the parameters of the experiment.

The different topology of these two cases can be highlighted by probing the trajectory of $g(k)$ in the complex plane: $|g(k)|$ is extracted from the measurement of the band structure, and the phase $\phi(k) = \arg[g(k)]$ is obtained by Fourier transforming the slow modulation of the output signal [34]. Figure 2(e) reports this slow modulation, as a function of time and k vector, for both the trivial and topological phases. Extracting the phase of this modulation at every k, we can track the trajectory of $g(k)$ throughout the entire Brillouin zone [Figs. 2(c)–2(d)], which winds around the origin in the topological case (d) but not in the trivial case (c).

Generalized SSH lattices.—We now examine the impact of 3rd-nearest-neighbor hopping amplitudes. In our platform, long-range hopping processes are straightforwardly implemented by adding appropriate higher-frequency

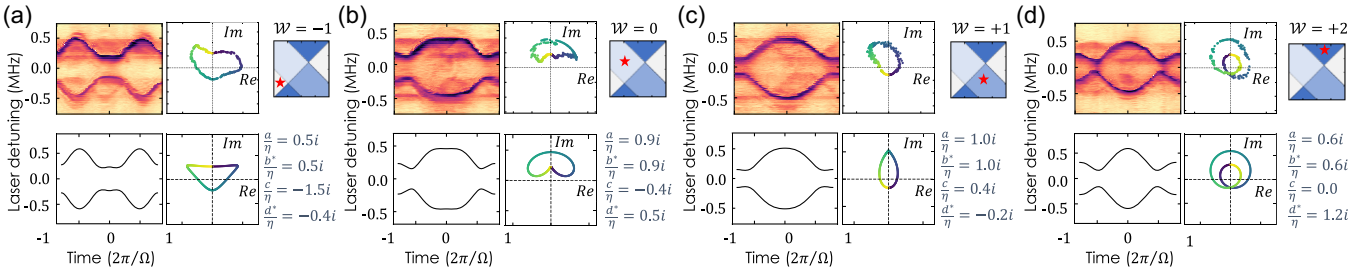

FIG. 3. Measurements (top row) and numerical simulations (bottom row) of the band structure (left column) and of the trajectory of $g(k)$ (central column) for dimer chains with long-range hopping amplitudes. Each panel shows results for each possible value of the winding number: $\mathcal{W} = -1$ (a), $\mathcal{W} = 0$ (b), $\mathcal{W} = +1$ (c), and $\mathcal{W} = +2$ (d). On the right side of each panel, we reproduce the phase diagram of Fig. 1(c), with a star indicating in which region of the phase diagram each measurement is realized, and provide the effective hopping amplitudes, normalized by η (in units of V).

components to the signal sent to the EOMs:

$$V_{\mathrm{CCW,CW}}(t) = \pm\frac{i}{2}(V_a e^{-i\delta t} + V_b e^{-i(\Omega-\delta)t} + V_c e^{-i(\Omega+\delta)t} + V_d e^{-i(2\Omega-\delta)t}) + \text{c.c.}, \quad (5)$$

where $c = -i\eta V_c$ and $d^* = -i\eta V_d^*$ [34]. Here we consider cases with $a = b^*$ and only the ratios c/a and d^*/a are changed. Keeping these ratios real, this allows exploring the full phase diagram presented in Fig. 1(c).

Figure 3 presents the experimental data for different ratios of long-range to nearest-neighbor hopping amplitudes. Each panel presents a specific case corresponding to one of the possible values of the winding number: $\mathcal{W} = -1$ (a), $\mathcal{W} = 0$ (b), $\mathcal{W} = +1$ (c), and $\mathcal{W} = +2$ (d). On the right of each panel, we present the effective hopping amplitudes used in the experiment. The experimental measurements of the band structure and trajectory of $g(k)$ (top row) show excellent agreement with tight-binding calculations (bottom row).

Time-reversal-breaking topological phases.—Finally, we demonstrate how the phases of the 3rd-nearest-neighbor couplings can be tuned to break time-reversal symmetry and induce a topological phase transition without modifying the hopping strengths. This is in sharp contrast with the conventional SSH model where it is necessary to adjust the coupling strengths to change $\mathcal{W}$, because any hopping phase can always be gauged away. This topological phase transition with fixed coupling strengths is allowed because these dimer chains with broken time-reversal symmetry belong to the *AIII* symmetry class rather than the *BDI* class to which the SSH model and its extensions with time-reversal symmetry belong.

The relative phase between the different hopping terms of the Hamiltonian is experimentally realized by adding a phase to $V_{a,b,c,d}$ in Eq. (5). Such a relative phase between one of the long-range couplings and the other couplings effectively induces a synthetic gauge field for photons [38,39]. This is best seen by reformulating the chain as a ladderlike lattice with $c = 0$ [Fig. 4(a)]. In this equivalent picture, one clearly sees how the phase of $d = |d|e^{-i\theta}$ gives rise to flux plaquettes similar to those in ladder models with a staggered magnetic field. This gauge field provides an additional degree of freedom, extending the phase diagram in Fig. 1(c) to three dimensions. A similar argument can of course be used when the c couplings are also included.

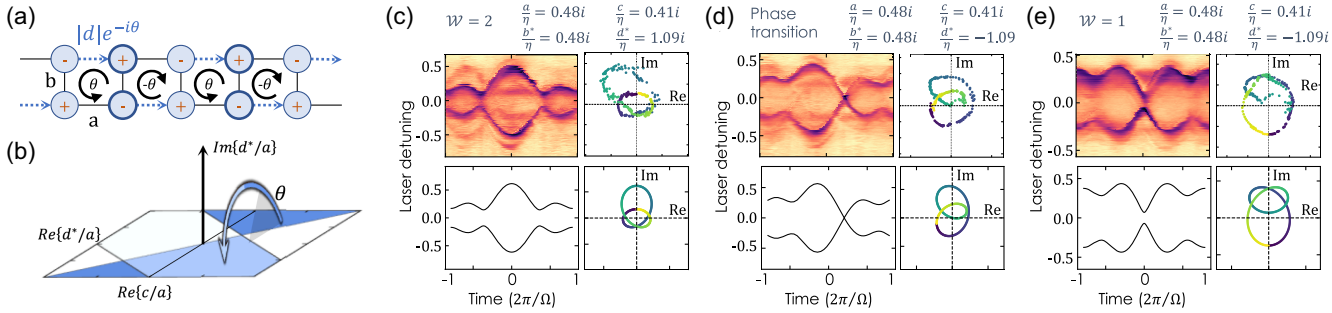

FIG. 4. (a) Schematic representation of a topological dimer chain with $a = b^*$, $c = 0$, and complex-valued d^*/a. The two sublattices are identified with + and − as in Fig. 1(e). (b) Schematic representation of the trajectory in the topological phase diagram followed by the Hamiltonian as the phase of the 3rd-nearest-neighbor hopping amplitudes (θ) is scanned. (c)–(e) Measurements of the band structure (top left) and $g(k)$ trajectory (top right) as the phase of the long-range hopping is tuned from $\theta = 0$ (c), to $\theta = \pi/2$ (d), and $\theta = \pi$ (e). The bottom row presents the corresponding theoretical calculation of the band structure (left) and $g(k)$ (right). For each panel, the effective hopping terms normalized by η are provided (in units of V).

An example of a trajectory in this extended phase space, that goes through points where the magnitude of all hopping amplitudes remains constant but the phase of d^*/a evolves from 0 to π, is schematically depicted in Fig. 4(b). Figures 4(c)–4(e) present the measured (top) and calculated (bottom) band structures (left) and trajectories of $g(k)$ (right) along this path. Once again, except for the small deviations observed in Figs. 4(d) and 4(e) near gap closures due to the finite decay rate γ [34], an overall excellent agreement is found between theory and experiment. A topological phase transition induced by this gauge field is clearly observed at $\theta = \pi/2$ through a closing and reopening of the energy gap accompanied by a winding number change from 2 to 1.

Conclusions.—In this work, we have exploited a synthetic dimension scheme based on an optical fiber loop to realize a generalized dimer chain model including long-range and/or time-reversal breaking hopping terms. Experimental signatures of the nontrivial band topology have been obtained by reconstructing the geometry of the Bloch wave functions throughout the entire Brillouin zone. The natural next step will be to relate this microscopic characterization of the topology to macroscopic observables such as a driven-dissipative version of the mean chiral displacement [14,31,40] and edge states in the presence of frequency-space potentials [14,41]. Setting up these tools will be instrumental in enabling investigations of more complex Hamiltonians in synthetic dimensions, involving non-Hermiticity [25,42], higher dimensions [43], many-body quantum states of light [44–46], non-Markovian dynamics [47], and/or optical nonlinearities [48,49].

Note added.—Recently, Ref. [50] demonstrating the extraction of the Zak phase of SSH lattices in the synthetic frequency dimension came to our attention.

P. S. J. acknowledges financial support from Québec's Minstère de l'Économie, de l'Innovation et de l'Énergie. P. S. J. and W. A. C. acknowledge financial support from the Fonds de Recherche–Nature et Technologies (FRQNT) and from the Natural Sciences and Engineering Research Council (NSERC). F. P. acknowledges financial support from FRQNT and R. H. from MITACS. I. C. acknowledges financial support from the Provincia Autonoma di Trento, from the Q@TN Initiative, and from the PNRR MUR project PE0000023-NQSTI. I. C. acknowledges financial support from the Provincia Autonoma di Trento, from the Q@TN Initiative, and from the PNRR MUR project PE0000023-NQSTI financed by the European Union–Next Generation EU. I. C. acknowledges continuous collaboration with Tomoki Ozawa and Greta Villa on this topic.

[1] B. Bradlyn, L. Elcoro, J. Cano, M. G. Vergniory, Z. Wang, C. Felser, M. I. Aroyo, and B. A. Bernevig, Nature (London) **547**, 298 (2017).
[2] F. D. M. Haldane, Phys. Rev. Lett. **61**, 2015 (1988).
[3] C. K. Chiu, J. C. Y. Teo, A. P. Schnyder, and S. Ryu, Rev. Mod. Phys. **88**, 035005 (2016).
[4] A. Bansil, H. Lin, and T. Das, Rev. Mod. Phys. **88**, 021004 (2016).
[5] E. Kapit and E. Mueller, Phys. Rev. Lett. **105**, 215303 (2010).
[6] R. Landig, L. Hruby, N. Dogra, M. Landini, R. Mottl, T. Donner, and T. Esslinger, Nature (London) **532**, 476 (2016).
[7] D. Jaksch, C. Bruder, J. I. Cirac, C. W. Gardiner, and P. Zoller, Phys. Rev. Lett. **81**, 3108 (1998).
[8] I. Bloch, J. Dalibard, and S. Nascimbène, Nat. Phys. **8**, 267 (2012).
[9] T. Ozawa and H. M. Price, Nat. Rev. Phys. **1**, 349 (2019).
[10] S. K. Kanungo, J. D. Whalen, Y. Lu, M. Yuan, S. Dasgupta, F. B. Dunning, K. R. Hazzard, and T. C. Killian, Nat. Commun. **13**, 1 (2022).
[11] A. Celi, P. Massignan, J. Ruseckas, N. Goldman, I. B. Spielman, G. Juzeliunas, and M. Lewenstein, Phys. Rev. Lett. **112**, 043001 (2014).
[12] T. Chalopin, T. Satoor, A. Evrard, V. Makhalov, J. Dalibard, R. Lopes, and S. Nascimbene, Nat. Phys. **16**, 1017 (2020).
[13] F. A. An, B. Sundar, J. Hou, X. W. Luo, E. J. Meier, C. Zhang, K. R. A. Hazzard, and B. Gadway, Phys. Rev. Lett. **127**, 130401 (2021).
[14] T. Ozawa, H. M. Price, N. Goldman, O. Zilberberg, and I. Carusotto, Phys. Rev. A **93**, 043827 (2016).
[15] A. Dutt, M. Minkov, Q. Lin, L. Yuan, D. A. Miller, and S. Fan, Nat. Commun. **10**, 1 (2019).
[16] X. W. Luo, X. Zhou, J. S. Xu, C. F. Li, G. C. Guo, C. Zhang, and Z. W. Zhou, Nat. Commun. **8**, 1 (2017).
[17] F. Cardano, A. D'Errico, A. Dauphin, M. Maffei, B. Piccirillo, C. De Lisio, G. De Filippis, V. Cataudella, E. Santamato, L. Marrucci, M. Lewenstein, and P. Massignan, Nat. Commun. **8**, 1 (2017).
[18] E. Lustig, S. Weimann, Y. Plotnik, Y. Lumer, M. A. Bandres, A. Szameit, and M. Segev, Nature (London) **567**, 356 (2019).
[19] A. Regensburger, C. Bersch, B. Hinrichs, G. Onishchukov, A. Schreiber, C. Silberhorn, and U. Peschel, Phys. Rev. Lett. **107**, 233902 (2011).
[20] A. Schreiber, K. N. Cassemiro, V. Potoček, A. Gábris, P. J. Mosley, E. Andersson, I. Jex, and C. Silberhorn, Phys. Rev. Lett. **104**, 050502 (2010).
[21] Q. Lin, L. Yuan, M. Xiao, and S. Fan, Optica **5**, 1396 (2018).
[22] O. Zilberberg, S. Huang, J. Guglielmon, M. Wang, K. P. Chen, Y. E. Kraus, and M. C. Rechtsman, Nature (London) **553**, 59 (2018).
[23] S. Weidemann, M. Kremer, T. Helbig, T. Hofmann, A. Stegmaier, M. Greiter, R. Thomale, and A. Szameit, Science **368**, 311 (2020).
[24] L. Xiao, T. Deng, K. Wang, G. Zhu, Z. Wang, W. Yi, and P. Xue, Nat. Phys. **16**, 761 (2020).
[25] K. Wang, A. Dutt, C. C. Wojcik, and S. Fan, Nature (London) **598**, 59 (2021).
[26] A. Schumer, Y. G. Liu, J. Leshin, L. Ding, Y. Alahmadi, A. U. Hassan, H. Nasari, S. Rotter, D. N. Christodoulides, P. LiKamWa, and M. Khajavikhan, Science **375**, 884 (2022).

[27] A. Steinfurth, I. Krešić, S. Weidemann, M. Kremer, K. G. Makris, M. Heinrich, S. Rotter, and A. Szameit, Sci. Adv. **8**, 7412 (2022).
[28] A. Senanian, L. G. Wright, P. F. Wade, H. K. Doyle, and P. L. McMahon, Nat. Phys. **19**, 1333 (2023).
[29] L. Fan, K. Wang, H. Wang, A. Dutt, and S. Fan, Sci. Adv. **9** (2023).
[30] W. P. Su, J. R. Schrieffer, and A. J. Heeger, Phys. Rev. Lett. **42**, 1698 (1979).
[31] M. Maffei, A. Dauphin, F. Cardano, M. Lewenstein, and P. Massignan, New J. Phys. **20**, 013023 (2018).
[32] A. D'Errico, F. Di Colandrea, R. Barboza, A. Dauphin, M. Lewenstein, P. Massignan, L. Marrucci, and F. Cardano, Phys. Rev. Res. **2**, 023119 (2020).
[33] C. Vega, M. Bello, D. Porras, and A. González-Tudela, Phys. Rev. A **104**, 053522 (2021).
[34] See Supplemental Material at http://link.aps.org/supplemental/10.1103/PhysRevLett.132.183802 for details on the setup and measurement protocol and a detailed derivation of the effective Hamiltonian, field amplitudes, and input-output relations.
[35] L. Yuan, A. Dutt, and S. Fan, APL Photonics **6**, 71102 (2021).
[36] A. Dutt, M. Minkov, I. A. Williamson, and S. Fan, Light Sci. Appl. **9**, 1 (2020).
[37] F. S. Piccioli, A. Szameit, and I. Carusotto, Phys. Rev. A **105**, 053519 (2022).
[38] J. Dalibard, F. Gerbier, G. Juzeliunas, and P. Öhberg, Rev. Mod. Phys. **83**, 1523 (2011).
[39] Tomoki Ozawa, Hannah M. Price, Alberto Amo, Nathan Goldman, Mohammad Hafezi, Ling Lu, Mikael C. Rechtsman, David Schuster, Jonathan Simon, Oded Zilberberg, and Iacopo Carusotto, Rev. Mod. Phys. **91**, 015006 (2019).
[40] G. Villa, I. Carusotto, and T. Ozawa, arXiv:2309.16101.
[41] A. Dutt, L. Yuan, K. Y. Yang, K. Wang, S. Buddhiraju, J. Vučković, and S. Fan, Nat. Commun. **13**, 3377 (2022).
[42] Z. Gong, Y. Ashida, K. Kawabata, K. Takasan, S. Higashikawa, and M. Ueda, Phys. Rev. X **8**, 031079 (2018).
[43] D. Cheng, E. Lustig, K. Wang, and S. Fan, Light Sci. Appl. **12**, 158 (2023).
[44] M. Lubasch, A. A. Valido, J. J. Renema, W. S. Kolthammer, D. Jaksch, M. S. Kim, I. Walmsley, and R. Garcia-Patron, Phys. Rev. A **97**, 062304 (2018).
[45] M. Bello, G. Platero, J. I. Cirac, and A. González-Tudela, Sci. Adv. **5**, eaaw0297 (2019).
[46] E. Kim, X. Zhang, V. S. Ferreira, J. Banker, J. K. Iverson, A. Sipahigil, M. Bello, A. González-Tudela, M. Mirhosseini, and O. Painter, Phys. Rev. X **11**, 011015 (2021).
[47] A. Ricottone, M. S. Rudner, and W. A. Coish, Phys. Rev. A **102**, 012215 (2020).
[48] T. Ozawa and I. Carusotto, Phys. Rev. Lett. **118**, 013601 (2017).
[49] N. Pernet, P. St-Jean, D. D. Solnyshkov, G. Malpuech, N. Carlon Zambon, Q. Fontaine, B. Real, O. Jamadi, A. Lemaître, M. Morassi, L. Le Gratiet, T. Baptiste, A. Harouri, I. Sagnes, A. Amo, S. Ravets, and J. Bloch, Nat. Phys. **18**, 678 (2022).
[50] G. Li, L. Wang, R. Ye, Y. Zheng, D. W. Wang, X. J. Liu, A. Dutt, L. Yuan, and X. Chen, Light Sci. Appl. **12**, 1 (2023).